The Astrophysical Journal, 950:51 (6pp), 2023 June 10 https://doi.org/10.3847/1538-4357/accc32

Anterograde Collisional Analysis of Solar Wind Ions

E. Johnson[1], B. A. Maruca[1], M. McManus[2], K. G. Klein[3], E. R. Lichko[4], J. Verniero[5], K. W. Paulson[6], H. DeWeese[1], I. Dieguez[6], R. A. Qudsi[7], J. Kasper[8], M. Stevens[6], B. L. Alterman[9], L. B. Wilson III[5], R. Livi[2], A. Rahmati[2], and D. Larson[2]
[1] Department of Physics and Astronomy, University of Delaware, Newark, DE 19716, USA; ejohn@udel.edu
[2] Department of Physics, University of California, Berkeley, CA 94720, USA
[3] Lunar and Planetary Laboratory, University of Arizona, Tucson, AZ 85721, USA
[4] Department of Astronomy and Astrophysics, University of Chicago, Chicago, IL 60637, USA
[5] NASA Goddard Space Flight Center, Heliophysics Science Division, Greenbelt, MD 20771, USA
[6] Center for Astrophysics, Harvard University, Cambridge, MA 02138, USA
[7] Department of Physics, Boston University, Boston, MA 02215, USA
[8] BWX Technologies Inc, Washington DC 20001, USA
[9] Space Science, Southwest Research Institute, San Antonio, TX 78238, USA
Received 2023 January 12; revised 2023 April 3; accepted 2023 April 7; published 2023 June 9

Abstract

Owing to its low density and high temperature, the solar wind frequently exhibits strong departures from local thermodynamic equilibrium, which include distinct temperatures for its constituent ions. Prior studies have found that the ratio of the temperatures of the two most abundant ions—protons (ionized hydrogen) and α-particles (ionized helium)—is strongly correlated with the Coulomb collisional age. These previous studies, though, have been largely limited to using observations from single missions. In contrast, this present study utilizes contemporaneous, in situ observations from two different spacecraft at two different distances from the Sun: the Parker Solar Probe (PSP; $r = 0.1$–0.3 au) and Wind ($r = 1.0$ au). Collisional analysis, which incorporates the equations of collisional relaxation and large-scale expansion, was applied to each PSP datum to predict the state of the plasma farther from the Sun at $r = 1.0$ au. The distribution of these predicted α–proton relative temperatures agrees well with that of values observed by Wind. These results strongly suggest that, outside of the corona, relative ion temperatures are principally affected by Coulomb collisions and that the preferential heating of α-particles is largely limited to the corona.

Unified Astronomy Thesaurus concepts: Solar wind (1534); Collision physics (2065); Plasma physics (2089)

1. Introduction

In any gas, neutral or ionized, collisions among constituent particles allow the exchange of momentum and energy; this shall gradually increase entropy and drive the system to a state of thermal equilibrium (Boltzmann 1868). The degree and rate of exchange of these parameters are determined by the configuration of the system. The collisions of interest are Coulomb collisions—"soft," small-angle deflections mediated by the electrostatic force (Livi et al. 1986). This can result in strong departures from local thermal equilibrium (LTE). When a medium is in LTE, the velocity distribution function (VDF) of each particle species is the entropically preferred Maxwell–Boltzmann distribution, and all particle species also have the same temperature and flow velocity at any given point in space (Griem 1963). In contrast, they frequently show temperature anisotropy (distinct temperatures along axes perpendicular and parallel to the magnetic field) and/or secondary populations (such as beams; Marsch & Goldstein 1983). Likewise, different ion species often have distinct temperatures and velocities.

The particles comprising the plasma of the solar wind do not have Maxwellian VDFs and are far from thermodynamic equilibrium. These non-Maxwellian features are a source of free energy and can drive energy transfer between the fields and the particles (Fitzpatrick 2014, 2020). Given the solar wind's low density and high temperature (Klein et al. 1985), the timescale over which Coulomb collisions significantly affect the plasma is very large. Indeed, this collisional timescale is often comparable to, or even much larger than, the transit time of the solar wind through the inner heliosphere (i.e., the expansion timescale; Verscharen et al. 2019). The solar wind's ions primarily consist of protons, with a few percent of α-particles (helium nuclei) and trace amounts of ions with heavier nuclei (Schmelz et al. 2012). Accounting for the solar wind's long collisional timescale, Coulomb collisions could act to erode non-LTE features within the solar wind, causing remnants of them to persist through much of the inner heliosphere and beyond (Livi et al. 1986). These non-LTE features result from extreme heating/acceleration processes that preferentially act on some particle species and/or along some directions (Marsch 2006).

The processes by which collisions bring ion temperatures—especially those of protons (T_p) and α-particles (T_α)—into LTE has received considerable attention in the study of the solar wind (see Section 3.3.1 of Verscharen et al. 2019 and references therein). In situ observations of near-Earth solar wind have shown that the α-proton relative temperature,

$$\theta_{\alpha p} \equiv \frac{T_\alpha}{T_p}, \tag{1}$$

varies widely (Verscharen et al. 2019), though typically $\theta_{\alpha p} \gtrsim 1$, which indicates a strong tendency for the preferential heating of α-particles relative to protons (Kasper et al. 2008).

Previous statistical studies (e.g., Neugebauer 1976; Von Steiger et al. 1995; Hefti et al. 1998; Kasper et al. 2008, 2017; Maruca et al. 2013; Tracy et al. 2016; Wilson et al. 2018; Kasper & Klein 2019) of measurements from single spacecraft (see Section 2) have provided strong evidence that after this initial preferential heating in/near the solar corona the value of $\theta_{\alpha p}$ changes primarily as a result of gradual collisional thermalization.

This work uses these ideas to find how the $\theta_{\alpha p}$ temperature ratio should evolve as a function of distance from the Sun. It is the first to analyze contemporaneous observations from two spacecraft at different distances from the Sun to directly test this hypothesis. This will allow us to estimate the initial thermal parameters of the distribution as it leaves the Sun, as well as evaluate the role that local kinetic processes play in the heating of ions in the solar wind. Section 2 gives an overview of prior studies of ion relative temperature and describes the theoretical framework for this present work. Section 3 presents a collisional analysis of measurements from the Parker Solar Probe (PSP), and Section 4 compares that analysis to observations from the Wind spacecraft. Concluding remarks are offered in Section 5.

2. Background

Variations in the α-proton relative temperature, $\theta_{\alpha p}$ (Equation (1)), have long been associated with the actions of Coulomb collisions (Neugebauer 1976). Previous studies have used the concept of the Coulomb number, N_c, alternatively referred to as collisional age, though Verscharen et al. (2019, Section 3.2.6) note that this usage has fallen out of favor:

$$N_c = \frac{r}{v_r \tau_c}, \tag{2}$$

where r is the distance from the Sun that an in situ measurement was made, v_r is the radial component of the solar wind velocity, and τ_c is the timescale for Coulomb collisional thermalization. The ratio r/v_r is approximately the expansion time of the plasma from the Sun to the observer, so N_c approximates the number of collisional timescales that have elapsed in that journey (Verscharen et al. 2019). Plasma with $N_c \gg 1$ indicates that heavy collisional processing has occurred, while $N_c \ll 1$ suggests that collisions have had little effect (Baumjohann & Treumann 1997). Statistical analyses from various spacecraft have revealed a strong, anticorrelation between $\theta_{\alpha p}$ and N_c (Feldman et al. 1974; Marsch et al. 1982; Kasper et al. 2008, 2017; Maruca et al. 2013; Tracy et al. 2015).

Though useful as a qualitative tool, the Coulomb number suffers from the tacit assumption that the plasma's bulk parameters remain fixed with distance from the Sun. Though this could arguably be the case with radial speed (v_r), the collisional timescales (τ_c) vary dramatically. Though formulae vary for τ_c depending on particular conditions, typically

$$\tau_c \propto \frac{T^{3/2}}{n}, \tag{3}$$

where T is temperature and n is density, both of which decrease with distance from the Sun (Hernández & Marsch 1985). To take into account the radial dependence of τ_c, some studies (Hernández et al. 1987; Chhiber et al. 2016; Kasper & Klein 2019) have utilized an integral form of the Coulomb number called the collisional age:

$$A_c(t) = \int_{t_0}^{t} \frac{dt'}{\tau_c(t')} = \int_{r_0}^{r} \frac{dr'}{v_r(r')\tau_c(r')}, \tag{4}$$

where t and t_0 are the limits for the time over which the collisions occur, which translate to the distances of r, representing the distance at which an observation is made, and r_0, representing the center of the heliosphere. In practice, this integral is carried out over r, where function forms of $n(r)$, $v_r(r)$, and $T(r)$ can be taken from empirical observations or simulations.

Both Coulomb number and collisional age focus on determining how extensively an individual parcel of solar wind plasma has been processed by Coulomb collisions. Maruca et al. (2013) introduced an alternative approach, since dubbed collisional analysis, which instead seeks to quantify how collisions affect the plasma's departures from LTE. That original study focused specifically on the α-proton relative temperature ($\theta_{\alpha p}$; Equation (1)) and carried out a "retrograde" collisional analysis, using a measurement of $\theta_{\alpha p}$ at $r = 1.0$ au to predict its value for $r = 0.1$ au (i.e., "undoing" the effects of collisions). The derived model gives the radial gradient in $\theta_{\alpha p}$ as

$$\frac{d\theta_{\alpha p}}{dr} = \left(\frac{An_p}{v_{rp}T_p^{3/2}}\right)\left(\frac{\mu_\alpha^{1/2}Z_\alpha^2(1-\theta_{\alpha p})(1+\eta_{\alpha p}\theta_{\alpha p})}{(\mu_\alpha+\theta_{\alpha p})^{3/2}}\right)\lambda_{\alpha p}, \tag{5}$$

where

$$\lambda_{\alpha p} = 9 + \ln\left[B\left(\frac{T_p^{3/2}(\mu_\alpha+\theta_{\alpha p})}{n_p^{1/2}Z_\alpha(1+\mu_\alpha)}\right)\left(1+\frac{Z_\alpha^2\eta_{\alpha p}}{\theta_{\alpha p}}\right)^{-1/2}\right]. \tag{6}$$

In these equations, $A = 2.60 \times 10^7\ \mathrm{cm^3\ km\ K^{3/2}\ s^{-1}\ au^{-1}}$, $B = 1\ \mathrm{cm^{-3/2}K^{-3/2}}$, $Z_\alpha \equiv q_\alpha/q_p = 2$ is the α-proton relative charge, $\mu_\alpha \equiv m_\alpha/m_p \approx 4$ is their relative mass, and $\eta_{\alpha p} \equiv n_\alpha/n_p$ is the their relative abundance. The value for $T_p^{3/2}$ derives from the rms speed between the two colliding species with charge state Z_α (Wilson et al. 2018). Though the value of $\eta_{\alpha p}$ varies widely in the solar wind, it typically has a value of a few percent (Marsch et al. 1982; Kasper et al. 2012; Alterman et al. 2018); this model assumed $\eta_{\alpha p}$ remained fixed within any given parcel of solar wind plasma as it expands through the heliosphere. In contrast, the model allows the other parameters to vary with r. In particular, Maruca et al. (2013) used the following radial scaling based on the analysis of Helios observations by Hellinger et al. (2011):

$$n_p(r) \propto r^{-1.8},\ v_{rp}(r) \propto r^{-0.2},\ \text{and}\ T_p(r) \propto r^{-0.74}. \tag{7}$$

This collisional analysis technique in Equation (5) was applied to 2.1 million measurements of the near-Earth solar wind in Maruca et al. (2013), in order to produce a prediction for observations closer to the Sun. This study is the first direct test of this prediction with an "anterograde" collisional analysis —one in which in situ measurements closer to the Sun are used to predict the state of the solar wind farther from the Sun.

3. Analysis

PSP (Fox et al. 2016) orbits the Sun in highly eccentric orbits that pass far closer to the Sun than any prior mission. During each of PSP's "encounters" with the Sun, its instruments directly sample the particles and fields of the nascent solar wind and even the solar corona (Kasper et al. 2021; Livi et al. 2021).

This study's primary data set was derived from PSP Encounters 4 (2020 January 23–February 3), 6 (2020 September 22–October 2), and 7 (2021 January 12–23), this being a result of available data. Each encounter began at a distance $r \approx 0.27$ au from the Sun, continued to a perihelion of about $r \approx 0.1$ au, and out to $r \approx 0.27$ au. Measurements of proton and α-particle densities, velocities, and temperatures were derived from the ion electrostatic analyzer (ESA) in PSP's SWEAP instrument suite (Kasper et al. 2016; Livi et al. 2021). Each ion spectrum that is fully or mostly observed from this instrument was fitted with a model consisting of three bi-Maxwellian VDFs: one each for the proton core, proton beam, and α-particle core. No α-particle beam data were available and thus not analyzed. Following the example of Maruca et al. (2013), we defined T_p and T_α to be the scalar temperature of the proton and α-particle cores, respectively. The scalar temperature of an ion species "i" is

$$T_i = \frac{2T_{i,\perp} + T_{i,\parallel}}{3}, \tag{8}$$

where $T_{i,\perp}$ and $T_{i,\parallel}$ are the temperature of the i-particles along the axes perpendicular and parallel to the ambient magnetic field. Though higher-order moments are required to fully describe ion distribution functions, $T_{i,\perp}$ and $T_{i,\parallel}$ are often sufficient to describe the cores of the distribution functions (Marsch et al. 2006).

Though the ESA's average measurement cadences during Encounters 6 and 7 were comparable (112 s and 125 s), its average measurement cadence during Encounter 4 was substantially faster (6.9 s). Though all the encounters were of approximately the same duration, Encounter 4 operated at a significantly higher cadence than the others. As a result, simply merging all encounters would have heavily biased the data set in favor of Encounter 4. To ensure that the encounters were roughly equally represented in the final data set, every 16 data points from Encounter 4 were averaged to produce an average measurement cadence (112 s), close to that of the other encounters, ensuring no bias in the final data set favoring a single Encounter and to achieve an equal number of data points from each encounter. Prior results without the application of averaging revealed a heavy bias in the data set toward Encounter 4, due to the significantly larger number of data points in that encounter. Encounters 6 and 7 contained approximately 7700 data entries, while Encounter 4 contained approximately 100,000 entries; after accounting for the cadence averaging the final data set contained 23,770 entries, roughly evenly split among the three encounters.

Figure 1 shows the probability distribution of α-proton relative temperature ($\theta_{\alpha p}$; Equation (1)) for this PSP data set. The data were sorted among 45 bins ranging from $\theta_{\alpha p} = 0$ to 10, the count of the number of data in each bin was divided by the total number of data, and the $\theta_{\alpha p}$-width of the bin to approximate probability density (Maruca et al. 2011).

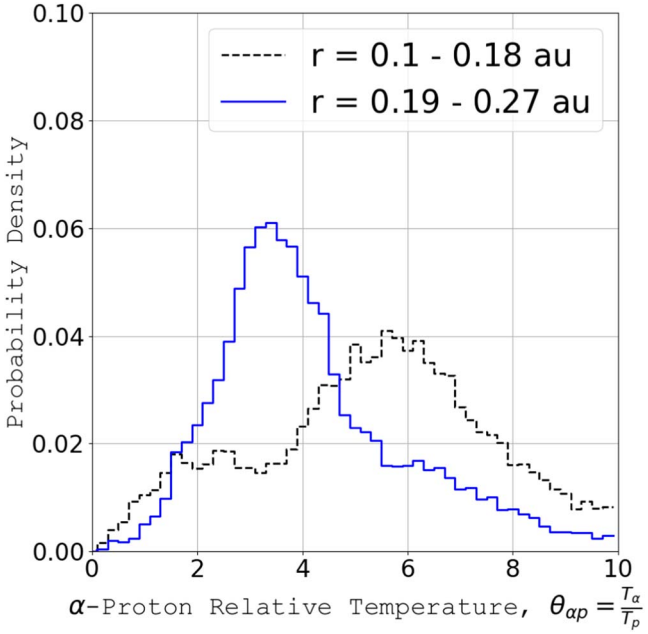

Figure 1. Histogram of observed values of $\theta_{\alpha p} \equiv \frac{T_\alpha}{T_p}$ from the PSP data set ($r = 0.1$ to 0.27 au). Bin counts have been normalized to approximate probability density (Section 3).

This PSP data set, like those from prior studies (Marsch et al. 1982; Kasper et al. 2008; Gershman et al. 2012) of the inner heliosphere, shows a strong tendency for α-particle temperature to exceed that of the protons. Indeed, $\theta_{\alpha p} > 1$ for 98% of the PSP data set. The underlying data span a range of distances ($r = 0.1$–0.27 au) rather than coming from a few specific distances, which would facilitate a more direct comparison. Additionally, observations were not uniformly distributed in r, with a mean r-value of 0.18 au. Even so, this range of radial distances is too small to effectively study the plasma's radial evolution.

The utility of Figure 1 for the study of collisional effects is limited. Particular care must be exercised in comparing the plot's two curves. Though Coulomb collisions are expected to be actively affecting ions in going from the region $r = 0.1$–0.18 au to the region $r = 0.19$–0.27 au, the solid blue curve in Figure 1 must not be regarded as the collisionally evolved version of the dashed black curve. Such a comparison might be possible for a sufficiently large data set, but all three PSP encounters used in this study span only about 30 days in total. In contrast, the corresponding plot by Maruca et al. (2013, their Figure 1) drew on over 15 yr of Wind measurements and thus may be regarded as less affected by variations among solar wind streams. Thus, each curve in Figure 1 was built up from only a few distinct solar wind streams, and the differences between the two curves represent a convolution of the effect of collisional thermalization and variations among streams. For example, Figure 1 does show that the average $\theta_{\alpha p}$-value is lower for $r = 0.19$–0.27 au and for $r = 0.1$–0.18 au. While this is consistent with the effects of collisions, $\theta_{\alpha p}$ does also vary considerably at a fixed r-value. Likewise, the dashed curve in Figure 1 does show what appears to be the beginnings of a bimodal distribution like that seen by Kasper et al. (2008) and Maruca et al. (2013)—here with a primary peak at $\theta_{\alpha p} \approx 6$ and a very weak secondary one at $\theta_{\alpha p} \approx 2$. Even so, it is difficult to determine whether this quasi-bimodal distribution is

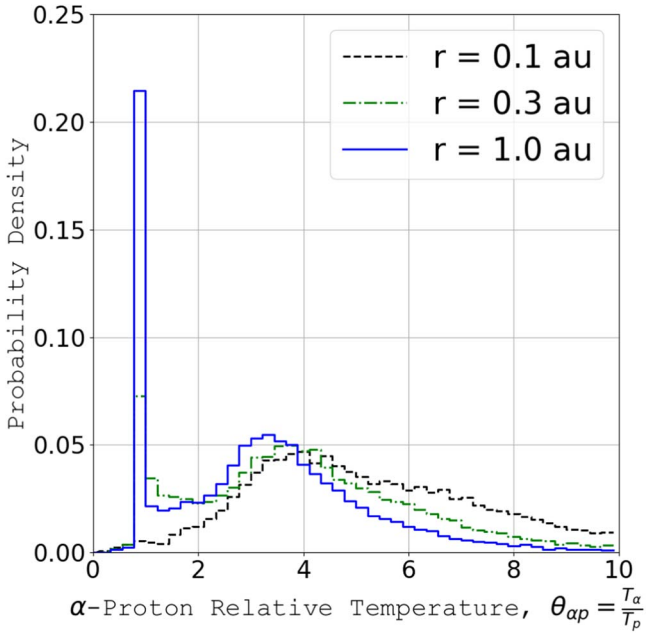

Figure 2. Histograms of the predicted $\theta_{\alpha p}$-values from the PSP data set based on collisional analyses extending the measured values to different heliocentric distances: $r = 0.1$ au (black dashed), 0.3 au (green dotted–dashed), and 1.0 au (blue solid).

due to the early effects of collisions or simply variations among the solar wind streams.

To address these issues, collisional analysis was applied to the measurements in the PSP data set. For this purpose, a "datum" from PSP was taken to consist of the set of values of v_p, n_p, $\eta_{\alpha p} = \frac{n_\alpha}{n_p}$, T_p, and $\theta_{\alpha p} = \frac{T_\alpha}{T_p}$ measured at a given distance r from the Sun. Each such datum was used as a boundary condition for Equation (5) to solve for the value of $\theta_{\alpha p}$ at some other "target" r-value. Though it was assumed that the α-proton abundance ratio, $\eta_{\alpha p}$, remained fixed during the expansion, n_p, v_p, and T_p were allowed to scale from their measured values according to the relationships in Equation (7). The differential equation in Equation (5) was solved numerically for each datum via Euler's method with 100 steps.

Figure 2 shows the results of this collisional analysis on the PSP data set for three different target distances from the Sun: $r = 0.1$, 0.3, and 1.0 au. The predicted $\theta_{\alpha p}$-values for each target r-value were binned and normalized in an identical manner to the measured $\theta_{\alpha p}$-values for Figure 1. For the target $r = 0.1$ au, the collisional analysis was "retrograde," i.e., Equation (5) was used, as by Maruca et al. (2013), to "undo" the effects of collisions on the plasma. In contrast, for $r = 0.3$ and 1.0 au, the collisional analysis was "anterograde," i.e., used to predict the further collisional evolution of the plasma. These observations are consistent with prior studies from Maruca et al. (2013), Kasper et al. (2008), and Wilson et al. (2018), which observed a double-peaked distribution from Wind with $\theta_{\alpha p} = 1.35$ and 3.49.

As r increases, the average value for $\theta_{\alpha p}$ decreases, and the formation of a secondary population takes place at $\theta_{\alpha p} \approx 1$, corresponding to LTE. In Figure 2, specifically for $r = 0.1$ au, there exists a predominate peak at $\theta_{\alpha p} \approx 4.2$. Corresponding peak values for $\theta_{\alpha p}$ at the target distances are presented in Table 1 and correspond to the first ($X_{25\%}$) and third ($X_{75\%}$) quartiles. The upper peak moves down as the secondary population forms, resulting in a prediction of a bimodal distribution at $r = 1.0$ au, which is consistent with prior analyses of 1.0 au observations by Kasper et al. (2008) and Maruca et al. (2013).

Table 1
Peaks of $\theta_{\alpha p}$ for the Probability Distributions in Figure 2

	Peaks of $\theta_{\alpha p}$	
r (au)	Lower	Upper
0.1	...	4.2
0.3	1.0	3.8
1.0	1.0	3.2

The peaks at $\theta_{\alpha p} \approx 1$ in the $r = 0.3$ and 1.0 au curves in Figure 2 must be regarded as artificially narrow. In Equation (5), the gradient in the α-proton temperature ratio ($d\theta_{\alpha p}/dr$) is the product of multiple factors, all of which are always strictly positive except one: $1 - \theta_{\alpha p}$. Consistent with thermodynamic expectations, this factor ensures that $\theta_{\alpha p}$ always converges to unity (i.e., local thermodynamic equilibrium) in the limit of large r. Even if the real distribution of $\theta_{\alpha p}$-values contained such a narrow peak, it would never be observed to be so narrow by actual in situ instruments due to their finite resolution and cadence. For example, Maruca et al. (2013) estimated just the random error (excluding systematic errors) in Wind Faraday cup measurements of T_α to be about 15% and T_p to be about 7%.

4. Comparison

To validate the PSP-derived prediction for the $r = 1.0$ au distribution of $\theta_{\alpha p}$-values, this study utilizes a secondary data set from the Wind spacecraft (Acuna et al. 1995), which orbits the Earth-Sun first Lagrange point (L1) at nearly $r = 1.0$ au (Wilson et al. 2018). Faraday cups were used to take in situ measurements of proton and α-particle parameters. These were derived from fits of ion spectra from Wind's Solar Wind Experiment (Ogilvie et al. 1995); these include but are not limited to density, speed, and ion temperature.

Wind data were selected to align with the PSP encounters, each of which occurred over 10 days. To account for the differences in heliographic longitude between Wind and PSP, the Wind data set was populated with measurements from a time period ranging from 10 days prior to each encounter to 10 days after Encounter 4 (2020 January 10–February 14), Encounter 6 (2020 September 10–October 14), and Encounter 7 (2020 December 30–2021 February 2). This resulted in 30 days (roughly one Carrington rotation) of continuous Wind measurements for each PSP encounter, giving 47,295 entries total. Figure 3 shows the distribution of $\theta_{\alpha p}$-values from the Wind data set, which was generated with identical binning and normalization to that of Figure 1. The Wind data are shown in red while the PSP-derived prediction for the 1 au $\theta_{\alpha p}$-distribution remains in blue from Figure 2.

The two 1.0 au $\theta_{\alpha p}$-distributions in Figure 3—one measured by Wind and the other predicted from contemporaneous PSP measurements closer to the Sun—reveal many qualitative similarities. Both are strongly bimodal with a taller but narrower peak at $\theta_{\alpha p} \approx 1$ and a shorter, broader peak at $\theta_{\alpha p} \approx 3$ (Table 2). The $\theta_{\alpha p} \approx 1$ peak predicted for $r = 1.0$ au from PSP data is significantly narrower than that measured at $r = 1.0$ au with Wind, but, as noted in Section 3, this is to be expected from the finite accuracy of instrument measurements.

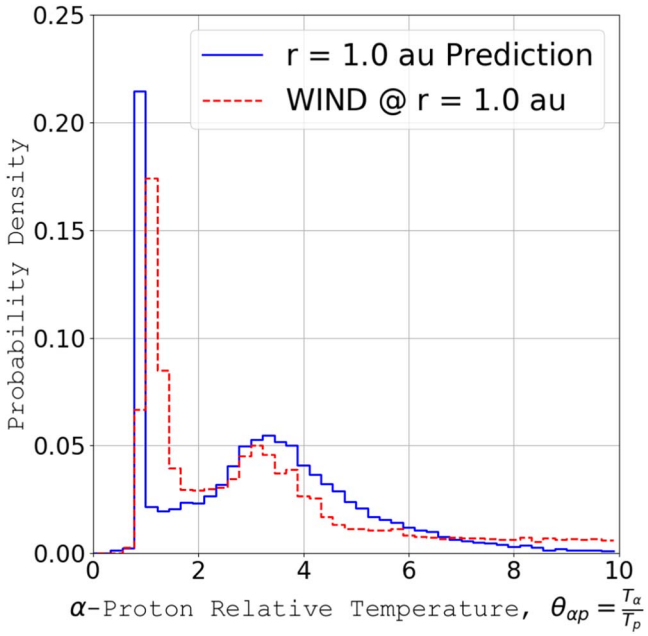

Figure 3. Histogram of predicted $\theta_{\alpha p}$-values from the PSP data set based on collisional analyses at $r = 1.0$ au (blue solid), compared to observed $\theta_{\alpha p}$-values from the Wind data set at $r = 1.0$ au (red dashed).

Table 2
Peaks of $\theta_{\alpha p}$ for the Probability Distributions in Figure 3

	r (au)	Upper $\theta_{\alpha p}$ Peak
Wind	1.0	3.0
Prediction	1.0	3.2

Both peaks have comparable values when compared to the predictions from Maruca et al. (2013) and Wilson et al. (2018), studies which used data sets comprising a larger number of entries.

5. Discussion

This study is the most direct test to date of the collisional analysis technique—the first to directly compare contemporaneous spacecraft at two different distances from the Sun. The similarities between the curves in Figure 3 suggest that the radial evolution of the $\theta_{\alpha p}$ through the inner heliosphere is dominated by the effects of Coulomb collisions. For this study, no preferential heating was incorporated into the collisional model (Equation (5)), instead assuming that thermalization from Coulomb collisions is the dominating factor when extending the PSP observations at $r \leqslant 0.27$ au to $r = 1.0$ au. Had the curves in Figure 3 shown significant discrepancies, it might have been concluded that some ongoing preferential heating occurs between $r = 0.27$ and 1.0 au. In actuality, the predicted and measured curves bear striking qualitative similarity: a trailing tail, bimodal distribution, sharp upper peak at $\theta_{\alpha p} \approx 1$ and broad lower peak at $\theta_{\alpha p} \approx 3$, all of which strongly suggests that preferential ion heating is largely confined to regions closer to the Sun, i.e., a majority of the T_α/T_p values are greater than 1 prior to this distance. This is consistent with prior predictions (Kasper et al. 2008, 2017; Maruca et al. 2013; Kasper & Klein 2019): the PSP's in situ observations of near-Sun solar wind reveals the near-ubiquitous preferential heating of α-particles over protons (i.e., $\theta_{\alpha p} \gg 1$; Figure 1).

Even so, for several reasons, the PSP prediction does not perfectly replicate the Wind measurements. An ideal test of collisional analysis would compare data taken simultaneously by two spacecraft in the same steady solar wind stream. For PSP and Wind, the two spacecraft were never actually radially aligned. Even when their heliographic longitudes were the same, they had distinct latitudes. Furthermore, no solar wind stream is ever truly steady, and this study has not accounted for any intrinsic error that may be present in the spacecraft observations. Though this can be partially compensated for by a statistically large data set consisting of measurements from many streams, the available PSP observations comprise only a few orbits of the spacecraft.

As the PSP mission progresses, the data set will grow substantially, which will allow for more exhaustive studies of collisional processes. In addition to expanding the robustness of the present result, future studies could also explore the effects of Coulomb collisions on other departures from LTE, including temperature anisotropy, differential flow, and multi-component VDFs (e.g., beams and cores).

E.J. and B.A.M. are partially supported by the NSF, award No. 1931435, E.R.L. was supported by NSF award No. 1949802. This research made use of PlasmaPy, a community-developed open-source Python package for plasma science PlasmaPy (2021). We acknowledge the NASA Parker Solar Probe Mission and Solar Wind Electrons Alphas and Protons (SWEAP) team led by Professor Justin Kasper, NASA contract NNN06AA01C.

Data from PSP are proprietary for a limited time and then accessible via Johns Hopkins Applied Physics Laboratory (Livi et al. 2020); Wind data can be downloaded from the CDAWeb, https://cdaweb.gsfc.nasa.gov/index.html/. Software relating to this project can also be found published on GitHub and is primarily programmed using Python, https://github.com/ejohnson-96/Collisionality. Additional scripts related to this research have been deposited to Zenodo by Johnson (2023).

Software: numpy (Harris et al. 2020), astropy (Astropy Collaboration et al. 2022), plasmapy (PlasmaPy 2021), matplotlib (Hunter 2007).

ORCID iDs

E. Johnson https://orcid.org/0000-0002-7326-1864
B. A. Maruca https://orcid.org/0000-0002-2229-5618
M. McManus https://orcid.org/0000-0001-6077-4145
K. G. Klein https://orcid.org/0000-0001-6038-1923
E. R. Lichko https://orcid.org/0000-0003-1945-8460
J. Verniero https://orcid.org/0000-0003-1138-652X
K. W. Paulson https://orcid.org/0000-0002-5699-090X
H. DeWeese https://orcid.org/0000-0002-8068-7740
I. Dieguez https://orcid.org/0000-0003-4988-2967
R. A. Qudsi https://orcid.org/0000-0001-8358-0482
J. Kasper https://orcid.org/0000-0002-7077-930X
M. Stevens https://orcid.org/0000-0002-7728-0085
B. L. Alterman https://orcid.org/0000-0001-6673-3432
L. B. Wilson III https://orcid.org/0000-0002-4313-1970
R. Livi https://orcid.org/0000-0002-0396-0547
A. Rahmati https://orcid.org/0000-0003-0519-6498
D. Larson https://orcid.org/0000-0001-5030-6030

References

Acuna, M. H., Ogilvie, K. W., Baker, D. N., et al. 1995, SSRv, 71, 5
Alterman, B. L., Kasper, J. C., Stevens, M. L., & Koval, A. 2018, ApJ, 864, 112
Astropy Collaboration, Price-Whelan, A. M., Lim, P. L., et al. 2022, ApJ, 935, 167
Baumjohann, W., & Treumann, R. A. 1997, Basic Space Plasma Physics (London: Imperial College Press)
Boltzmann, L. 1868, Studien über das Gleichgewicht der lebendigen Kraft zwischen bewegten materiellen Punkten (Wiener Berichte) (Vienna: K. und k. Hof- und Staatsdr.)
Chhiber, R., Usmanov, A., Matthaeus, W., & Goldstein, M. 2016, ApJ, 821, 34
Feldman, W. C., Asbridge, J. R., & Bame, S. J. 1974, JGR, 79, 2319
Fitzpatrick, R. 2014, Plasma Physics: An Introduction (Boca Raton, FL: CRC Press)
Fitzpatrick, R. 2020, Thermodynamics and Statistical Mechanics (Singapore: World Scientific)
Fox, N. J., Velli, M. C., Bale, S. D., et al. 2016, SSRv, 204, 7
Gershman, D. J., Zurbuchen, T. H., Fisk, L. A., et al. 2012, JGRA, 117, A00M02
Griem, H. R. 1963, PhRv, 131, 1170
Harris, C. R., Millman, K. J., van der Walt, S. J., et al. 2020, Natur, 585, 357
Hefti, S., Grünwaldt, H., Ipavich, F. M., et al. 1998, JGRA, 103, 29697
Hellinger, P., Matteini, L., Štverák, v., Trávníček, P. M., & Marsch, E. 2011, JGRA, 116, A09105
Hernández, R., Livi, S., & Marsch, E. 1987, JGRA, 92, 7723
Hernández, R., & Marsch, E. 1985, JGRA, 90, 11062
Hunter, J. D. 2007, CSE, 9, 90
Johnson, E. 2023, Collisional Analysis v1.1, Zenodo, doi:10.5281/zenodo.7822610
Kasper, J. C., Abiad, R., Austin, G., et al. 2016, SSRv, 204, 131
Kasper, J. C., & Klein, K. G. 2019, ApJL, 877, L35
Kasper, J. C., Klein, K. G., Lichko, E., et al. 2021, PhRvL, 127, 255101
Kasper, J. C., Klein, K. G., Weber, T., et al. 2017, ApJ, 849, 126
Kasper, J. C., Lazarus, A. J., & Gary, S. P. 2008, PhRvL, 101, 261103
Kasper, J. C., Stevens, M. L., Korreck, K. E., et al. 2012, ApJ, 745, 162
Klein, L. W., Ogilvie, K. W., & Burlaga, L. F. 1985, JGR, 90, 7389
Livi, R., Larson, D. E., Kasper, J. C., et al. 2021, Earth Space Sci.
Livi, R., Larson, D. E., & Rahmati, A. 2020, PSP Solar Wind Electrons Alphas and Protons (SWEAP) SPAN-A Proton Distribution Function, Partial Moments, Instrument Frame, Level 3 (L3), 7 s Data, doi:10.48322/ypyh-s325
Livi, S., Marsch, E., & Rosenbauer, H. 1986, JGR, 91, 8045
Marsch, E. 2006, LRSP, 3, 1
Marsch, E., & Goldstein, H. 1983, JGRA, 88, 9933
Marsch, E., Mühlhäuser, K.-H., Rosenbauer, H., Schwenn, R., & Neubauer, F. M. 1982, JGRA, 87, 35
Marsch, E., Zhao, L., & Tu, C.-Y. 2006, AnGeo, 2057, 24
Maruca, B. A., Bale, S. D., Sorriso-Valvo, L., Kasper, J. C., & Stevens, M. L. 2013, PhRvL, 111, 241101
Maruca, B. A., Kasper, J. C., & Bale, S. D. 2011, PhRvL, 107, 201101
Neugebauer, M. 1976, JGR, 81, 78
Ogilvie, K. W., Chornay, D. J., Fritzenreiter, R. J., et al. 1995, SSRv, 71, 55
PlasmaPy, C. 2021, PlasmaPy, version v0.6.0, Zenodo, doi:10.5281/zenodo.4602818
Schmelz, J. T., Reames, D. V., von Steiger, R., & Basu, S. 2012, ApJ, 755, 33
Tracy, P. J., Kasper, J. C., Raines, J. M., et al. 2016, PhRvL, 116, 255101
Tracy, P. J., Kasper, J. C., Zurbuchen, T. H., et al. 2015, ApJ, 812, 170
Verscharen, D., Klein, K. G., & Maruca, B. A. 2019, LRSP, 16, 5
Von Steiger, R., Geiss, J., Gloeckler, G., & Galvin, A. B. 1995, SSRv, 72, 71
Wilson, L. B., III, Stevens, M. L., Kasper, J. C., et al. 2018, ApJS, 236, 41